Ultrashort echo time magnetic resonance elastography for quantification of the mechanical properties of short T2 tissues via optimal control-based radiofrequency pulses

Pilar Sango-Solanas, Kevin Tse Ve Koon, Eric van Reeth, Stéphane Nicolle, Jean-françois Palierne, Cyrielle Caussy, Olivier Beuf

Ultra short echo time MR Elastography for the mechanical properties quantification of short T2 tissues via Optimal Control-based RF pulses

Pilar Sango-Solanas[1], Kevin Tse Ve Koon[1], Eric Van Reeth[1,2], S. Nicolle[3], JF. Palierne[4], Cyrielle Caussy[5,6] and Olivier Beuf[1]

[1]Univ Lyon, INSA-Lyon, Inserm, UCBL1, CNRS, CREATIS, UMR 5220, U1294, F-69621 Villeurbanne, France

[2]CPE Lyon, Département Sciences du Numérique, Lyon, France

[3]Univ Lyon, Univ Gustave Eiffel, Univ Claude Bernard Lyon 1, LBMC UMR_T 9406, F-69622, Lyon, France

[4]École Normale Supérieure de Lyon, CNRS, UMR 5672, Laboratoire de Physique, F-69342, France

[5]Univ Lyon, CarMen Laboratory, INSERM, INRA, INSA Lyon, Université Claude Bernard Lyon 1,69495 Pierre-Bénite, France

[6]Hospices Civils de Lyon, Département Endocrinologie, Diabète et Nutrition, Hôpital Lyon Sud, 69495 Pierre-Bénite, France

Word count: 5359

Key words: MR Elastography, Optimal Control theory, RF pulse design, short T2, tendon.

Corresponding author:
Pilar SANGO-SOLANAS, PhD
CREATIS CNRS UMR 5220
INSA Lyon, Bât Léonard de Vinci
21 Avenue Jean Capelle
F-69621 Villeurbanne, FRANCE
Tél. +33 4 72 43 85 20
Pilar.sango@creatis.univ-lyon1.fr

List of abbreviations

DENSE, Displacement ENcoding with Stimulated Echoes

G', shear storage modulus

GRAPE, GRadient Ascent Pulse Engineering

MEG, Motion Encoding Gradient

MRE, Magnetic Resonance Elastography

OC, Optimal Control

PMP, Pontryagin Maximum Principle

PNR, Phase to Noise Ratio

RARE, Rapid Acquisition with Refocused Echoes)

RF, Radiofrequency

ROI, Region of Interest

SNR, Signal to Noise Ratio

UTE, Ultra short Echo Time

Summary abstract (274/300)

Purpose: To demonstrate the feasibility of RF pulses generated via an Optimal Control (OC) algorithm to perform Magnetic Resonance Elastography (MRE) and quantify the mechanical properties of materials with very short transverse relaxation times (T2<5ms) for the first time.
Methods: Optimal Control theory applied to MRE provides RF pulses that bring isochromats from the equilibrium state to a fixed target state, which corresponds to the phase pattern of a conventional MRE acquisition. Such RF pulses applied with a constant gradient, allow to simultaneously perform slice selection and motion encoding in the slice direction. Unlike conventional MRE, no additional motion encoding gradients (MEG) are needed enabling shorter echo times. OC pulses were implemented both in turbo spin echo (OC RARE) and Ultrashort Echo-time (OC UTE) sequences to compare their motion encoding efficiency with the conventional MEG encoding (classical MEG MRE). MRE experiments were carried out on agar phantoms with very short T2-values and on an *ex vivo* bovine tendon.
Results: Magnitude images, wave field images, Phase to Noise Ratio (PNR) and shear storage modulus maps were compared between OC RARE, OC UTE and classical MEG MRE in samples with different T2 values. Shear storage modulus values of the agar phantoms were in agreement with values found in the literature and that of the bovine tendon was corroborated with rheometry measurements.
Conclusion: Only the OC sequences could encode motion in very short T2 samples and only OC-UTE sequences yielded magnitude images enabling proper visualization of short T2 samples and tissues. The OC UTE sequence produced the best PNRs, demonstrating its ability to perform anatomical and mechanical characterization. Its success warrants *in vivo* confirmation on further studies.

1. Introduction (1101)

The characterization of biological tissues with short transverse relaxation times (T2) is an actual challenge in the field of Magnetic Resonance Imaging (MRI). Indeed, some tissues having T2 of the order of the millisecond or less can be found in the human body in organs such as bones[1,2], tendons[3,4], lungs[5] or in tissues with strong concentrations of iron oxydes[6]. To obtain anatomical images of such tissues with MRI, several dedicated pulse sequences that enable short echo times have been developed[7]. One of them is the UTE (Ultra Short echo time) sequence, in which a radial readout with spokes starting from the center of the k-space is used[8]. Most MRI applications are interested in magnitude images, to which different contrast weightings can be applied depending on the organs to be visualized. However, phase images can also contain useful information about the characteristics of tissues in some MRI applications such as the phase contrast mechanism called Magnetic Resonance Elastography (MRE).

MRE was developed in the late 1990s and since then, it has been studied by several research groups. MRE is a non-invasive imaging technique that allows the quantification of mechanical properties of biological tissues based on the physical characteristics of shear waves propagating through the examined tissues[9]. Several diseases altering the elasticity or viscosity of some organs or tissues can be quantified by MRE[10]. This allows the staging and longitudinal follow up of the disease to monitor its progression or regression. The main clinical application of MRE is the staging of liver fibrosis[11–14]. Other MRE studies have investigated the benefit of MRE in the examination of heart[15,16], brain[17,18], breast[19,20] and lungs[21,22], each of them having specific constraints to deal with.

A classical MRE sequence is characterized by the presence of oscillating motion encoding gradients (MEG) that are synchronized with external mechanical excitation and allow the encoding of nuclear spins motion into the phase of the NMR signal[9]. MEGs are defined by their amplitude and their frequency that is limited by the slew rate of the MRI scanner gradient system. Any MR pulse sequence can be easily adapted to MRE by inserting the oscillating gradients between the RF excitation and the signal acquisition. In the literature, the principal sequences such as turbo spin echo[23–25], gradient echo[26,27] and echo planar imaging[28] have been successfully used to perform MRE. In all the MRE sequences, the minimum echo time TE is largely dependent of the duration of MEGs. As they usually oscillate at the same frequency as the mechanical excitation, the echo time depends on the vibration frequency. Common MRE applications carried out on patient in clinical systems use vibrations ranging between 20 and 100 Hz, which corresponds to minimum TEs between 20 and 60 ms. This results in degraded

signals on samples having short transverse relaxation times. Therefore, with the classical motion encoding strategy, short T2 tissues cannot be mechanically quantified with a sufficient Phase-to-Noise Ratio (PNR) or within a reasonable scan time. For instance, it was demonstrated that the T2 shortening induced by iron overload on liver is a predictor of non-diagnostic MRE[29,30]. Short TEs would therefore be crucial for MRE feasibility on hemochromatosis patients.

Various innovative motion encoding strategies have been proposed to reduce the echo time. Fractional encoding proposes to encode a fraction of the motion period by using high frequency MEGs to encode low frequency vibrations[31]. The MEG period is smaller than the excitation wave period, allowing shorter TEs. But a trade-off is required between the encoded phase and the signal to noise ratio (SNR). A displacement encoding with stimulated echoes (DENSE) MRE sequence was also proposed[32,33]. This sequence consists in partially encoding motion before RF excitation and completing the encoding with a short gradient independent of the motion period. The echo time is thus reduced at the expenses of a loss of signal amplitude. Despite the reduction of echo times, both above-mentioned strategies apply encoding gradients between the excitation and the acquisition. Therefore, the limitation to short T2 tissues is not completely overcome. More recently, a study proposed a Motion-Sensitizing magnetization Preparation (MSPrep) pulse including motion encoding gradients to separate the motion encoding scheme from the image encoding[34]. At the end of the preparation pulse, the displacement information is kept on the longitudinal magnetization and any MR pulse sequence can be applied after to record the motion propagation in the magnitude images. Very short echo times can be achieved, especially with a UTE sequence. However, with this strategy, the resulting signal intensity is multifactorial since T1 and T2 weightings are also involved.

Instead of using MEGs, RF field gradients have been also investigated to encode motion[35–38]. It was first demonstrated that with a pattern of RF field gradients it is possible to detect the slow flow of a fluid[35]. Then, this idea was pushed forward to make spectroscopic elastography[36]. Optimal Control (OC) theory has been recently demonstrated to be a useful tool to optimize RF pulses able to control the magnetization phase[38]. Such pulses, in the presence of a constant gradient, can simultaneously perform spatially selective excitation and motion encoding[39]. The OC pulse brings isochromats from the equilibrium state to the desired target state, which corresponds to the phase pattern of a conventional MRE image. OC pulses can easily be inserted in any MR pulse sequence and because oscillating gradients are not required after excitation, this approach is compatible with very short echo times. This motion encoding strategy was demonstrated in a preliminary study with a RARE (Rapid Acquisition with

Refocused Echoes) sequence on samples with T2 values typical of liver tissues ranging from 20-30 ms[39]. It was shown that the OC strategy is able to maximize both the encoded phase and the SNR. Later, another study demonstrated the use of OC RF pulses to simultaneously encode a dual-frequency shear wave at short TE[40]. In view of the potential applications of OC pulses, the strategy has been further investigated to improve and broaden its applications. In this paper, we present the latest developments of OC theory applied to MRE: OC pulses are optimized to encode motion in short T2-values samples (<5ms) and added to a UTE sequence. The UTE sequence uses a radial mapping of k-space from the center, enabling echo times shorter than the RARE sequence. Both OC RARE and OC UTE sequences are compared to the classical MEG MRE sequence in terms of motion encoding efficiency. Agar phantoms doped with $MnCl_2$ and a bovine tendon are used for *in vitro* and *ex vivo* MRE experiments respectively. Our aim is to demonstrate the ability of Optimal Control MRE to quantify the mechanical properties of short T2 tissues.

2. Materials and methods (1787)

2.1 Optimal Control theory

Optimal Control theory computes the control parameter of a dynamic system with respect to a defined target state and its associated cost function through the application of the Pontryagin Maximum Principle (PMP)[41]. The optimal control problem is solved here with a numerical approach called GRAPE (GRadient Ascent Pulse Engineering) that was initially introduced for Nuclear Magnetic Resonance pulse design[42]. The GRAPE algorithm updates the control parameter and the trajectories that satisfy the optimal conditions to minimize the cost function at each iteration, while satisfying the constraints imposed by the PMP.

The considered dynamic system is the macroscopic magnetization $\vec{M}$ of isochromats, whose evolution is governed by Bloch equations:

$$\frac{d}{dt}\begin{pmatrix} M_x \\ M_y \\ M_z \end{pmatrix} = \begin{pmatrix} -\frac{1}{T_2} & \Delta B_0 & -u_y \\ -\Delta B_0 & -\frac{1}{T_2} & u_x \\ u_y & -u_x & -\frac{1}{T_1} \end{pmatrix} \begin{pmatrix} M_x \\ M_y \\ M_z \end{pmatrix} + \begin{pmatrix} 0 \\ 0 \\ \frac{M_0}{T_1} \end{pmatrix} \quad (1)$$

where ΔB_0 is the resonance offset and $\vec{U} = (u_x, u_y)$ is the control parameter corresponding to the RF pulse which will control the macroscopic magnetization from a given steady state to the defined target state. Only the x-component of the RF pulse is considered here[39]. Both the target states and the cost function are defined by the user depending on the desired application.

2.2 Optimal Control applied to MRE

OC applied to MRE has been well described[39]. The parameters defined to solve the OC problem applied to MRE are illustrated in Figure 1. The temporal evolution of the Bloch equations is discretized, to compute the magnetization at each time step. The parameters appearing in Bloch equations such as the relaxation times and the resonance offset must be defined. Indeed, the relaxation times are taken into account during the optimization process. This is crucial in the case of short transverse relaxation times since the loss of phase coherence can no longer be neglected during the application of the excitation pulse. In order to define the resonance offset, the spatial discretization has to be addressed first. The RF pulse is going to be applied with a constant gradient G_z to simultaneously perform slice selection and motion encoding while the

shear wave propagates through the sample. The concept of bandwidth Δf_{in} of the optimized RF pulse is thus achieved by discretizing J isochromats located at $z_{(j)}$ along the desired slice direction (taken to be z here). The slice thickness Δz_{in} is then fixed by the constant gradient amplitude and pulse bandwidth. Two outbands (Δz_{out}) are also considered beyond the slice thickness to limit the transverse magnetization outside the slice. Then, to account for the controlled fluctuation of the B_0 field perceived by the isochromats due to the oscillatory motion induced by the shear wave, isochromats are also discretized along the shear wave propagation direction (arbitrary chosen to be x). Each isochromat is located along the wavelength λ at $x_{(i)}$ with a motion initial phase given by $\theta_{(i)} = 2\pi \frac{x_{(i)}}{\lambda}$. Only two isochromats separated by a quarter of a wavelength ($\theta_{(1)} = 0$ and $\theta_{(2)} = \pi/2$) are considered here since it was demonstrated to be sufficient to converge towards a pulse able to encode motion throughout the whole wavelength while reducing the computation time[38].

Finally, the B_0 field variation perceived by isochromats located at (i, j) is finally given by:

$$\Delta B_{0_{(i,j)}}(t) = G_z\left(A \cdot sin\left(2\pi f t + \theta_{(i)}\right) + z_{(j)}\right) \quad (2)$$

where A and f represent the amplitude and the frequency of the shear wave respectively.

The target states are defined so as to minimize the transverse magnetization in the outbands and to maximize it inside the slice. In addition, the magnetization phase of in-slice isochromats is related to the isochromat phase in the oscillatory motion. The target states are thus described by:

$$\vec{T}_{(i,j)} = \left(\sin(\cos\theta_{(i)}), \cos\left(\cos\theta_{(i)}\right), 0\right) \quad if \quad z_{(j)} \in \Delta z_{in}$$

$$\vec{T}_{(i,j)} = (0,0,1) \quad if \quad z_{(j)} \in \Delta z_{out} \quad (3)$$

The cost function seeks to minimize the quadratic difference between the final states after the application of the pulse $\vec{M}_{(i,j)}(t_f)$ and the defined target states $\vec{T}_{(i,j)}$:

$$C(U) = \sum_{j=1}^{J} \sum_{i=1}^{2} \left\| \vec{M}_{(i,j)}\left(t_f\right) - \vec{T}_{(i,j)} \right\|^2 \quad (4)$$

2.3 MRE setup

MRI acquisitions were performed on a preclinical 7T BioSpec scanner (Bruker Biospin, Ettlingen, Germany), with a quadrature 72 mm inner diameter volume coil in transmit/receive mode. *In vitro* experiments were carried on agar (2%wt) phantoms doped with Manganese chloride $MnCl_2$. The phantom was a bi-layer cube with 1 and 5 mM $MnCl_2$ concentrations. *Ex*

vivo experiments were carried on a bovine tendon embedded in an agar (2.6%wt) cube in such a way that the tendon fibers were positioned vertically, perpendicular to the magnetic field B_0. Relaxation times measured using a RARE (Rapid Acquisition with Refocused Echoes) sequence with different TEs and TRs were $[T1, T2]_{1mM} = [66.4\pm1, 3.4\pm0.3]$ ms, $[T1, T2]_{5mM} = [28.9\pm1.2, 1.3\pm0.4]$ ms for the phantom. The tendon had heterogeneous relaxation time values varying from 400 to 1200 ms and from 8 to 12 ms for the T1 and T2, respectively. A piezoelectric actuator (CEDRAT Technologies) was used as mechanical transducer driver. A waveform generator (Agilent 33220A) was configured to produce the shear wave signals.

2.4 OC pulses implementation details

Pulses were numerically optimized for two different excitation frequencies of 300 and 600 Hz. The lower limit was chosen so as to have suitable wavelengths with respect to the small size of the phantoms. The upper limit was chosen so as to restrict wave attenuation which increases with frequency while also ensuring a sufficiently long wavelength with respect to the inplane voxel size. Given the very short targeted T2, different optimized pulse durations were tested and among the multiple solutions generated, the best pulses generated at each excitation frequency were considered for experimental tests. Further details of the optimization parameters of both OC pulses used for the tests are summarized in Table 1. The following parameters were common to all the pulses. The pulse amplitudes $|u_x|$ were bounded to 94 μT in order to respect the constraints of the coil and the RF amplifier. The slice bandwidths Δf_{in} were set to 7 kHz, which corresponds to a 1mm slice with a gradient amplitude Gz=164 mT/m. The outer bandwidth intervals were set to $\pm$[4.5,10.5] kHz yielding a transition band of ±[3.5, 4.5] kHz. The frequency steps were set to $f_{step_{in}}$ = 10 Hz and $f_{step_{out}}$ = 20 Hz in the slice and the outer bandwidth, respectively. Only two isochromats groups per wavelength (at $\theta_{(1)} = 0$ and $\theta_{(2)} = \pi/2$) were considered. This yields a total of 2002 (=2 types of isochromats * ($\Delta f_{in}/f_{step_{in}}$ +1) + 2 outbands *($\Delta f_{out}/f_{step_{out}}$)) different isochromats that were simulated and controlled per pulse. The computation time for each pulse was around 12 h on a computing grid of 4-core, 2.5 GHz machines.

2.5 MRE acquisitions

Classical MEG MRE and OC-based MRE sequences were carried out on both phantoms. For the classical method, a RARE sequence was used with a low turbo factor of 4. A single cycle of sinusoidal MEG of 164 mT/m amplitude was added before and after the first refocusing

pulse. MEG was synchronized with the mechanical excitation and its frequency was equal to the vibration frequency in each acquisition. The OC RF pulses were inserted as excitation pulses in RARE[40] (turbo factor = 4) and UTE (402 spokes) sequences (see Figure 2). The OC pulse itself was synchronized with the mechanical excitation. Since the OC approach implies that motion has to be aligned with the constant gradient, motion was sensitized in a single direction, corresponding to the slice direction. For the tendon tissue, it was oriented so as to have its fibers aligned within the selected slice. Axial slices of 1 mm thickness were acquired. The TE was fixed to the minimum possible for each sequence. Four equally-spaced phase offsets were acquired. To avoid artifacts during the viscoelastic parameters reconstruction, the excitation frequencies were adapted to each phantom so that there were at least one and a half wavelength encoded in the propagation direction and that a wavelength contained at least nine voxels[43]. Further details of the acquisition parameters for each phantom are summarized in Table 2.

The wave generator was triggered at the beginning of each TR to reach a steady-state wave propagation before the beginning of the MR sequences. Two acquisitions with inversion of the wave polarity were done for phase images subtraction and removal of static phase offsets. Acquisitions without motion were also carried out to compute the phase noise.

2.6 Image analysis

2.6.1 G' reconstruction

Raw phase images were unwrapped with a quality guided path following phase unwrapping algorithm[44]. The proportional 2D displacement fields were calculated. Then, a directional filter was applied in the main propagation direction (from bottom to top) and the temporal Fourier transform was applied to the displacement fields. The first harmonic was kept for the viscoelastic parameters reconstruction. Then, spatial fourth-order 2D Butterworth filters with lower and upper thresholds of 0.3 and 1.5 cm^{-1} were applied to filter and preserve the wavelengths of interest as much as possible[11,45]. The spatial filter limits were chosen based on simulations of estimated wavelength values with different cut-offs filters values (data not shown). The Helmholtz equation inversion algorithm[10,46] was applied to the filtered displacement fields to calculate the shear storage modulus G' at each frequency, assuming a density of 1000 kg/m^3. Finally, a 3x3 median filter was applied to the elastograms.

ROIs were manually drawn excluding the phantom borders and regions where the wave propagation was not sufficient. The mean and standard deviation of G' were computed inside the ROIs.

2.6.2 PNR computation

The Phase-to-Noise ratio (PNR) is calculated to evaluate and compare the motion encoding efficiency of the different sequences on the phantom. The phase encoding is defined as the difference of the maximal and minimal phase encoded in a same pixel along time. Then, the PNR is defined as the ratio between the average value (over all pixels inside the ROI) of the phase encoding in presence of mechanical excitation (Δ) and the phase noise, defined as the average value of the phase encoding in the absence of motion (σ): $PNR=\Delta/\sigma$.

2.7 Rheometry measurements

In order to corroborate the shear storage modulus value of the bovine tendon found by MRE, rheometry measurements were carried out with a high-frequency rheometer[47,48] three days after MRE experiments. A disc-shaped axial section of the tendon with a diameter of 15 mm and a 1.5 mm thickness was contained between two glass plates mounted on a piezoelectric actuator. The top plate was driven vertically by the piezoelectric element in a small sinusoidal motion (~nm) with a frequency varying between 1 and 630 Hz, the small motion warranting that the measurements are independent on the strain and only dependent on the frequency. A squeeze flow was thus induced in the sample and the stress transmitted to the second plate was measured by the other piezoelectric ceramic. The complex modulus, and then the shear storage modulus, were directly deduced from the pressure applied by the sample on the sensor and the amplitude of motion[49]. As the sample was an axial slice of the tendon, the induced stress was perpendicular to the tendon fibers, resulting in the measurement of the G' in the same direction as in the MRE experiments.

3. Results (1021)

3.1 OC pulses in the simulation framework

3.1.1 OC pulses validation

To make a first validation of the performance of the OC pulses, the final states and the slice profile can be calculated by simulating through Bloch equations the application of the pulse to a numerical phantom with the same parameters as the optimization. The pulse B (see table 1) is considered here for the illustration of the OC pulses characteristics, presented in Figure 3. Figure 3A shows the simulated slice profile, calculated by integrating the transverse magnetization inside pixels aligned along the slice gradient direction. It reasonable fits to the desired slice thickness of 1 mm. Figure 3B presents the final states of the transverse magnetization in the transverse plane of the Bloch sphere of all the isochromats considered in the optimization process. The 0 and π/2 phase isochromats are perfectly distinct. We can define the simulated encoded phase as the difference between the mean phase of each isochromat ($\varphi_{sim} = \varphi_{sim_{iso\ \pi/2}} - \varphi_{sim_{iso\ 0}}$). Ideally, it should be equal to π/2 but in this case, it is smaller due to the short T2-values considered.

3.1.2 Robustness to the T2 variability

As OC pulses are optimized for a given T2, ideally the T2 of the studied sample has to be known *a priori* to adapt the T2 for the pulse optimization, which is sometimes not possible. The robustness of OC pulses to the variability of T2 is evaluated here by simulation to demonstrate the performance of OC pulses when having heterogeneous T2 samples such as tendons. To this end, the OC pulse B was applied through Bloch equations on several numerical phantoms with different T2 values. To simulate the effect of the OC pulse when there is no mechanical excitation, the pulse was also applied to the same numerical phantoms with a null motion amplitude. Figure 4 shows the obtained results. Figure 4A and 4B present the final states and the slice profiles on two numerical phantoms of T2 values of 1 and 20 ms with and without motion. When there is no mechanical excitation, no phase is encoded since the two isochromats population behave similarly (like if both had an initial phase of 0). The simulated phase noise σ_{sim} can be defined as the standard deviation of the isochromats phase in the absence of motion. The slice profile is nearly unchanged and so the obtained transverse magnetization amplitude is the same with and without motion for the same T2. From the figures, we can observe that the transverse magnetization amplitude is lower respectively higher if the sample T2-values are higher respectively lower to the optimized one. Results are

quantified and presented in Figure 4C, which shows the simulated encoded phase, the phase noise and the transverse magnetization amplitude with varying T2 values of the sample. Finally, the PNR, defined as the ratio of the simulated encoded phase divided by the phase noise ($\varphi_{sim}/\sigma_{sim}$), were computed and are shown in Figure 4D. PNR has the maximum value when T2=$T2_{opt}$ and decreases very slightly when T2>$T2_{opt}$. However, an abrupt decrease is noticed when T2<$T2_{opt}$.

3.2 Phantom acquisitions

Figure 5 shows the magnitude and phase images as well as the obtained elastograms of the phantom with the different sequences at 600 Hz. The layer with the concentration of 5 mM of $MnCl_2$ (i.e. the lowest 1ms T2-value) is only visible in magnitude images obtained with the OC UTE sequence since it has the shortest echo time. But the shear waves are encoded with both the OC RARE and OC UTE sequences.

The classical MEG MRE method is compared to the OC strategy in terms of phase encoding and PNR through the different acquisitions at two frequencies. Results are summarized in Figure 6A-B. Note that vertical axes are presented in logarithmic scales to enable the comparison among all acquisitions.

In the 5 mM $MnCl_2$ concentration layer (Figure 6A), the classical MEG sequences at both frequencies have long TEs compared to T2 so no signal can be acquired. Only the OC strategy allows a phase encoding, obtaining best PNRs with the OC UTE sequence.
In the 1 mM $MnCl_2$ concentration layer (Figure 6B), the classical MEG sequence only gives a signal at 600 Hz and the layer can therefore not be characterized at 300 Hz. At 600 Hz, the classical MEG and OC RARE sequences present higher phase encodings however the resulting PNRs are higher with the OC UTE.
Finally, the mean values and standard deviation of the shear storage modulus G' obtained for both excitation frequencies with the different sequences are presented in Figure 6C-D for the 5 mM and the 1 mM $MnCl_2$ concentration layers, respectively. An unexpected decrease of the shear modulus with increasing $MnCl_2$ concentration can be noticed.

3.3 **Tendon *ex vivo* acquisitions**

Figure 7 shows the results obtained on the bovine tendon at an excitation frequency of 600 Hz. Classical MEG and OC RARE sequences had too long echo times compared to the transverse

relaxation time of the tendon, yielding weak signals. Figures 7A-B-C display the magnitude images obtained with the classic MEG MRE, the OC RARE and the OC UTE sequences, respectively. Again, OC RARE and OC UTE showed propagating shear waves on phase images but only OC UTE led both magnitude images with sufficient SNR and phase images usable to reconstruct the G'. Figure 7D shows the phase image obtained with the OC UTE sequence. An increased wavelength is detected where the tendon is located. This implies a high shear storage modulus, which can also be seen in the elastogram in Figure 7E. The mean and standard deviation values of G' calculated in the ROI were 128 ± 26 kPa.

3.4 **Tendon rheometry measurements**

Figure 8 shows rheometry results. The shear storage modulus of tendon has a power law behavior. Data was fitted to a frequency power law model according to $G' \sim f^{\alpha}$ where f represents the motion frequency and α the exponent. The fit was done whit a non linear least squares method on Matlab ($R^2 = 0.9836$). The obtained exponent was 0.1147. The value of shear storage modulus at 600 Hz obtained by interpolation is 183 kPa.

4. Discussion (1171)

This article presents the advances in the application of the Optimal Control theory to MRE: the quantification of the mechanical properties of tissues having very short transverse relaxations times. This method is based on the use of RF pulses, designed with an optimal control algorithm, able to simultaneously perform slice selection and motion encoding, allowing signal acquisitions right after the RF pulse and so enabling short echo times. This is the main advantage compared to the classical MRE method, which applies motion encoding gradients between the excitation and the signal acquisition to encode motion, resulting in long echo times, especially for low frequency vibrations. The performance of the OC pulses was already validated on usual T2 samples[39,50]. In this study, we built upon these previous results to improve and adapt the OC algorithm to short T2-values in order to explore new applications of the OC MRE strategy.

Compared to the existing MRE strategies proposed in the literature to reduce the TE, the OC approach does not use motion encoding gradients before or after the pulse excitation (like the DENSE sequence[32] and the fractional encoding[31]) and as it is classically done, it encodes the motion in phase images (unlike the MSPrep strategy[34]). The OC strategy is thus the first method able to encode motion on the magnetization phase of isochromats with very short transverse relaxation times. From figure 3B, we can observe that the final transverse magnetization is about 50% of the theoretical maximum. However, in theory if we compute the signal obtained from a sample with a transverse relaxation time equal to the one of the optimization pulse B ($T2_{opt_B} = 2$ ms) at a time t=τ_B=5 ms, we obtain a final transverse magnetization of about 8%. This demonstrates the ability of OC pulses to partially compensate the effect of very short transverse relaxation times during its application thanks to the consideration of relaxation times throughout the optimization process.

One advantage of the OC strategy rests upon the flexibility of the algorithm. Indeed, in the optimization process we can consider any experimental imperfection. For example, several isochromats with different oscillating frequencies can be considered to perform simultaneous multifrequency MRE[40]. In addition, here we demonstrated by simulation the robustness of OC pulses to the sample T2 variability: OC pulse are robust when the actual T2 is longer than the optimized one and even when T2s are slightly smaller than the optimized value, the OC pulse is still able to fulfill correct phase encoding but transverse magnetization rapidly decreases. This means that an OC pulse optimized for the minimum possible T2 could be used in a

relatively wide range of T2s. This would facilitate the use of the OC strategy on clinical setups since just a few pulses could be sufficient for different applications.

According to the results, the classical MEG MRE sequence cannot quantify mechanical properties of very short T2 tissues since the echo times are prolonged by the presence of MEGs. On the other hand, the OC strategy can do it. Even if the magnitude images obtained with the OC RARE show a week signal in the 5 mM $MnCl_2$ concentration layer and the tendon (Figure 5 and 7B, respectively), the wave propagation is still encoded. From phantom results, we can notice that despite leading to lower encoded phase values, the reason for which will be investigated in future studies, the OC UTE sequence produces the highest PNRs at both excitation frequencies since phase noise are also reduced. PNRs are higher at 600 Hz than at 300 Hz. This could present an advantage compared to the classical MEG sequence which needs oscillating gradients that cannot reach high frequencies due to slew rate limitations. Moreover, being able to perform MRE at high frequencies is especially positive for the application on small and stiff tissues such as tendons.

Shear storage modulus values found on the agar phantoms are consistent with the literature[51] even though the difference of G' with $MnCl_2$ concentration was unexpected. However, to our knowledge there are no reported values of G' of tendons on the MRE literature. Hence, we carried out rheometry measurements on the tendon to corroborate the shear storage modulus obtained by MRE[52]. Both results were of the same order of magnitude (128 vs 183 kPa by MRE and rheometry, respectively) and were consistent since tendons are known to be quite stiff[53–55]. The difference between them could be explained by the fact that rheometry measurements are localized and with fiber orientations that might differ slightly from MRE measurements.

The OC UTE sequence is therefore the only method that allows the characterization of mechanical and anatomical properties from phase and magnitude images, respectively, of very short T2 tissues. Indeed, even averaged, the RARE sequence would not produce a sufficient SNR to consider a reliable reconstruction of viscoelastic parameters[56] nor a significant improvement of PNR. Nevertheless, the principal drawback of the OC UTE sequence is the longer acquisition time since many spokes are needed to respect the Nyquist theorem for a good reconstruction. Moreover, due to how the OC problem has been defined, the magnetization has still to return to the thermodynamic equilibrium state ($\vec{M} = (0,0,1)$) after each repetition so long TRs are needed. One possibility to reduce the repetition time would be

to further consider during the optimization process an equilibrium state different from the thermodynamic equilibrium. The acquisition time could then be reduced.

Currently, a limitation of the OC strategy is that only oscillatory motion vibrating in the same direction as the constant gradient can be encoded. Research is underway to extend the application of the strategy to the encoding of 3D motion. We are also exploring the adaptation of OC pulses to clinical MRE. Indeed, the constraints of clinical systems (maximum gradient amplitude and slew rate and maximum RF power amplitude) and the parameters used in clinical MRE (motion excitation frequency and amplitude…) are different from those of preclinical MRE. In particular, the energy deposited by the pulses must be sufficiently low to comply with accepted SAR levels. These challenges will be addressed in further works.

Finally, the application of MRE to quantify mechanical properties of short T2-values tissues is challenging. Some of the biological tissues having short T2 that have demonstrated to suffer from mechanical properties variations caused by diseases are lungs[57] and tendons[58]. Some patients can also have short T2 liver values when presenting high iron liver content in cases such as hemochromatosis[29]. While MRE was successfully carried on human lung parenchyma with a fractional encoding MRE sequence[21], tendons have not been investigated by MRE yet. Ultrasound elastography studies showed that Achilles tendinopathy induces a softening of the Achilles tendon (AT) tissues[58,59] and several MRI studies demonstrated that UTE sequences are more adapted than conventional Cartesian sequences for an early detection of abnormalities of the AT[8,60]. Hence, being able to obtain important anatomical information with an UTE sequence while characterizing its mechanical properties with the proposed OC UTE sequence could be a useful tool for the investigation of tendon diseases. High concentration iron livers could also benefit from the short echo times obtained with the OC strategies to enable a better mechanical characterization and thus simplifying patient's follow up.

5. Conclusion (192)

This article proposes a MRE strategy to mechanically characterize tissues having short transverse relaxation times. RF pulses designed with an Optimal Control algorithm are able to simultaneously perform slice selection and motion encoding. Motion encoding gradients being no longer needed, k-space readout can occur just after the excitation pulse and thus very short echo times obtained. This strategy was combined with both an accelerated spin echo (RARE) and an ultra-short echo time (UTE) sequence. Both sequences were successfully applied on short T2 samples, allowing the reconstruction of shear storage modulus maps. Results demonstrated that the OC UTE sequence produced better PNR. The OC UTE sequence could be a valuable tool to explore the anatomy and the mechanical properties of biological tissues having short T2 tissues. Future work will keep on the development of the optimal control algorithm to study the possibility of using a different equilibrium state in order to reduce the repetition time and so accelerate the acquisition. Finally, preclinical *in vivo* studies would be further carried out on a high concentration iron liver mouse model to analyze the pertinence of OC pulses of quantifying the mechanical properties of such tissues.

Acknowledgements (87)

This work was performed within the framework of the LabEx PRIMES of University of Lyon (ANR-11-LABX-0063), within the program "Investissements d'Avenir" (ANR-11-IDEX-0007) operated by the French National Research Agency (ANR). MR experiments were acquired on the PILoT platform, member of the France Life Imaging infrastructure (ANR-11-INBS-0006). A CC-BY public copyright license has been applied by the authors to the present document and will be applied to all subsequent versions up to the Author Accepted Manuscript arising from this sub-mission, in accordance with the grant's open access conditions.

Conflict of interest

The authors declare that they have no competing interests.

References

1. Reichert ILH, Robson MD, Gatehouse PD, He T, Chappell KE, Holmes J, Girgis S, Bydder GM. Magnetic resonance imaging of cortical bone with ultrashort TE pulse sequences. *Magn Reson Imaging*. 2005;23(5):611-618. doi:10.1016/j.mri.2005.02.017

2. Wehrli FW. Magnetic resonance of calcified tissues. *J Magn Reson*. 2013;229:35-48. doi:10.1016/j.jmr.2012.12.011

3. Gatehouse PD, Bydder GM. Magnetic Resonance Imaging of Short T2 Components in Tissue. *Clin Radiol*. 2003;58(1):1-19. doi:10.1053/crad.2003.1157

4. Robson MD, Benjamin M, Gishen P, Bydder GM. Magnetic resonance imaging of the Achilles tendon using ultrashort TE (UTE) pulse sequences. *Clin Radiol*. 2004;59(8):727-735. doi:10.1016/j.crad.2003.11.021

5. Hatabu H, Alsop DC, Listerud J, Bonnet M, Gefter WB. T2* and proton density measurement of normal human lung parenchyma using submillisecond echo time gradient echo magnetic resonance imaging. *Eur J Radiol*. 1999;29(3):245-252. doi:10.1016/S0720-048X(98)00169-7

6. Anderson LJ, Holden S, Davis B, Prescott E, Charrier CC, Bunce NH, Firmin DN, Wonke B, Porter J, Walker JM, Pennell DJ. Cardiovascular T2-star (T2*) magnetic resonance for the early diagnosis of myocardial iron overload. *Eur Heart J*. 2001;22(23):2171-2179. doi:10.1053/euhj.2001.2822

7. Weiger M, Pruessmann KP. Short-T2 MRI: Principles and recent advances. *Prog Nucl Magn Reson Spectrosc*. 2019;114-115:237-270. doi:10.1016/j.pnmrs.2019.07.001

8. Robson MD, Gatehouse PD, Bydder M, Bydder GM. Magnetic resonance: an introduction to ultrashort TE (UTE) imaging. *J Comput Assist Tomogr*. 2003;27(6):825-846. doi:10.1097/00004728-200311000-00001

9. Muthupillai R, Lomas D, Rossman P, Greenleaf J, Manduca A, Ehman R. Magnetic resonance elastography by direct visualization of propagating acoustic strain waves. *Science*. 1995;269(5232):1854-1857. doi:10.1126/science.7569924

10. Manduca A, Oliphant TE, Dresner MA, Mahowald JL, Kruse SA, Amromin E, Felmlee JP, Greenleaf JF, Ehman RL. Magnetic resonance elastography: Non-invasive mapping of tissue elasticity. *Med Image Anal*. 2001;5(4):237-254. doi:10.1016/S1361-8415(00)00039-6

11. Yin M, Talwalkar JA, Glaser KJ, Manduca A, Grimm RC, Rossman PJ, Fidler JL, Ehman RL. Assessment of Hepatic Fibrosis With Magnetic Resonance Elastography. *Clin Gastroenterol Hepatol*. 2007;5(10):1207-1213.e2. doi:10.1016/j.cgh.2007.06.012

12. Rouvière O, Yin M, Dresner MA, Rossman PJ, Burgart LJ, Fidler JL, Ehman RL. MR Elastography of the Liver: Preliminary Results. *Radiology*. 2006;240(2):440-448. doi:10.1148/radiol.2402050606

13. Hsu C, Caussy C, Imajo K, Chen J, Singh S, Kaulback K, Le MD, Hooker J, Tu X, Bettencourt R, Yin M, Sirlin CB, Ehman RL, Nakajima A, Loomba R. Magnetic Resonance vs Transient Elastography Analysis of Patients With Nonalcoholic Fatty Liver Disease: A Systematic Review and Pooled Analysis of Individual Participants. *Clin Gastroenterol Hepatol*. 2019;17(4):630-637.e8. doi:10.1016/j.cgh.2018.05.059

14. Huwart L, Sempoux C, Vicaut E, Salameh N, Annet L, Danse E, Peeters F, ter Beek LC, Rahier J, Sinkus R, Horsmans Y, Van Beers BE. Magnetic Resonance Elastography for the Noninvasive Staging of Liver Fibrosis. *Gastroenterology*. 2008;135(1):32-40. doi:10.1053/j.gastro.2008.03.076

15. Sack I, Rump J, Elgeti T, Samani A, Braun J. MR elastography of the human heart: Noninvasive assessment of myocardial elasticity changes by shear wave amplitude variations. *Magn Reson Med*. 2009;61(3):668-677. doi:10.1002/mrm.21878

16. Kolipaka A, Araoz PA, McGee KP, Manduca A, Ehman RL. Magnetic resonance elastography as a method for the assessment of effective myocardial stiffness throughout the cardiac cycle. *Magn Reson Med*. 2010;64(3):862-870. doi:10.1002/mrm.22467

17. Kruse SA, Rose GH, Glaser KJ, Manduca A, Felmlee JP, Jack CR, Ehman RL. Magnetic resonance elastography of the brain. *NeuroImage*. 2008;39(1):231-237. doi:10.1016/j.neuroimage.2007.08.030

18. Green MA, Bilston LE, Sinkus R. In vivo brain viscoelastic properties measured by magnetic resonance elastography. *NMR Biomed*. 2008;21(7):755-764. doi:https://doi.org/10.1002/nbm.1254

19. Sinkus R, Tanter M, Xydeas T, Catheline S, Bercoff J, Fink M. Viscoelastic shear properties of in vivo breast lesions measured by MR elastography. *Magn Reson Imaging*. 2005;23(2):159-165. doi:10.1016/j.mri.2004.11.060

20. McKnight AL, Kugel JL, Rossman PJ, Manduca A, Hartmann LC, Ehman RL. MR Elastography of Breast Cancer: Preliminary Results. *Am J Roentgenol*. 2002;178(6):1411-1417. doi:10.2214/ajr.178.6.1781411

21. Mariappan YK, Glaser KJ, Hubmayr RD, Manduca A, Ehman RL, McGee KP. MR elastography of human lung parenchyma: Technical development, theoretical modeling and in vivo validation. *J Magn Reson Imaging*. 2011;33(6):1351-1361. doi:10.1002/jmri.22550

22. Marinelli JP, Levin DL, Vassallo R, Carter RE, Hubmayr RD, Ehman RL, McGee KP. Quantitative assessment of lung stiffness in patients with interstitial lung disease using MR elastography. *J Magn Reson Imaging*. 2017;46(2):365-374. doi:10.1002/jmri.25579

23. Klatt D, Hamhaber U, Asbach P, Braun J, Sack I. Noninvasive assessment of the rheological behavior of human organs using multifrequency MR elastography: a study of brain and liver viscoelasticity. *Phys Med Biol*. 2007;52(24):7281-7294. doi:10.1088/0031-9155/52/24/006

24. Asbach P, Klatt D, Schlosser B, Biermer M, Muche M, Rieger A, Loddenkemper C, Somasundaram R, Berg T, Hamm B, Braun J, Sack I. Viscoelasticity-based Staging of Hepatic Fibrosis with Multifrequency MR Elastography. *Radiology*. 2010;257(1):80-86. doi:10.1148/radiol.10092489

25. Sango-Solanas P, Tse Ve Koon K, Ratiney H, Millioz F, Caussy C, Beuf O. Harmonic wideband simultaneous dual-frequency MR Elastography. *NMR Biomed*. 2021;34(2):e4442. doi:10.1002/nbm.4442

26. Venkatesh SK, Yin M, Glockner JF, Takahashi N, Araoz PA, Talwalkar JA, Ehman RL. MR Elastography of Liver Tumors: Preliminary Results. *Am J Roentgenol*. 2008;190(6):1534-1540. doi:10.2214/AJR.07.3123

27. Garteiser P, Sahebjavaher RS, Ter Beek LC, Salcudean S, Vilgrain V, Van Beers BE, Sinkus R. Rapid acquisition of multifrequency, multislice and multidirectional MR elastography data with

a fractionally encoded gradient echo sequence: MULTIFREQUENCY MRE WITH GRADIENT ECHOES. *NMR Biomed*. 2013;26(10):1326-1335. doi:10.1002/nbm.2958

28. Asbach P, Klatt D, Hamhaber U, Braun J, Somasundaram R, Hamm B, Sack I. Assessment of liver viscoelasticity using multifrequency MR elastography. *Magn Reson Med*. 2008;60(2):373-379. doi:10.1002/mrm.21636

29. Ghoz HM, Kröner PT, Stancampiano FF, Bowman AW, Vishnu P, Heckman MG, Diehl NN, McLeod E, Nikpour N, Palmer WC. Hepatic iron overload identified by magnetic resonance imaging-based T2* is a predictor of non-diagnostic elastography. *Quant Imaging Med Surg*. 2019;9(6):921-927. doi:10.21037/qims.2019.05.13

30. Wagner M, Corcuera-Solano I, Lo G, Esses S, Liao J, Besa C, Chen N, Abraham G, Fung M, Babb JS, Ehman RL, Taouli B. Technical Failure of MR Elastography Examinations of the Liver: Experience from a Large Single-Center Study. *Radiology*. 2017;284(2):401-412. doi:10.1148/radiol.2016160863

31. Rump J, Klatt D, Braun J, Warmuth C, Sack I. Fractional encoding of harmonic motions in MR elastography. *Magn Reson Med*. 2007;57(2):388-395. doi:10.1002/mrm.21152

32. Robert B, Sinkus R, Gennisson JL, Fink M. Application of DENSE-MR-elastography to the human heart. *Magn Reson Med*. 2009;62(5):1155-1163. doi:10.1002/mrm.22124

33. Strasser J, Haindl MT, Stollberger R, Fazekas F, Ropele S. Magnetic resonance elastography of the human brain using a multiphase DENSE acquisition. *Magn Reson Med*. 2019;81(6):3578-3587. doi:10.1002/mrm.27672

34. Boucneau T, Fernandez B, Darrasse L, Maître X. Prepared MR Elastography. In: *Proc Int Soc Magn Reson Med; 2021; Abstract 30*.

35. Karczmar GS, Tweig DB, Lawry TJ, Matson GB, Weiner MW. Detection of motion using B1 gradients. *Magn Reson Med*. 1988;7(1):111-116. doi:https://doi.org/10.1002/mrm.1910070113

36. Baril N, Lewa CJ, de Certaines JD, Canioni P, Franconi JM, Thiaudière E. MR Detection of Mechanical Vibrations Using a Radiofrequency Field Gradient. *J Magn Reson*. 2002;154(1):22-27. doi:10.1006/jmre.2001.2451

37. Turk E, Ider YZ, Ergun AS, Demir T, Atalar E. Shear Wave Imaging by using B1 gradients. In: *Proc Int Soc Magn Reson Med; 2013; Abstract 0015*.

38. Lefebvre PM, Van Reeth E, Ratiney H, Beuf O, Brusseau E, Lambert SA, Glaser SJ, Sugny D, Grenier D, Tse Ve Koon K. Active control of the spatial MRI phase distribution with optimal control theory. *J Magn Reson*. 2017;281:82-93. doi:10.1016/j.jmr.2017.05.008

39. Van Reeth E, Lefebvre PM, Ratiney H, Lambert SA, Tesch M, Brusseau E, Grenier D, Beuf O, Glaser SJ, Sugny D, Tse-Ve-Koon K. Constant gradient elastography with optimal control RF pulses. *J Magn Reson*. 2018;294:153-161. doi:10.1016/j.jmr.2018.07.013

40. Sango Solanas P, Tse Ve Koon K, Van Reeth E, Ratiney H, Millioz F, Caussy C, Beuf O. Short echo time dual-frequency MR Elastography with Optimal Control theory. In: *Proc Int Soc Magn Reson Med; 2021; Abstract 1029*.

41. Pontryagin LS. *Mathematical Theory of Optimal Processes*. Wiley; 1962.

42. Khaneja N, Reiss T, Kehlet C, Schulte-Herbrüggen T, Glaser SJ. Optimal control of coupled spin dynamics: design of NMR pulse sequences by gradient ascent algorithms. *J Magn Reson*. 2005;172(2):296-305. doi:10.1016/j.jmr.2004.11.004

43. Mura J, Schrank F, Sack I. An analytical solution to the dispersion-by-inversion problem in magnetic resonance elastography. *Magn Reson Med*. 2020;84(1):61-71. doi:https://doi.org/10.1002/mrm.28247

44. Ghiglia DC, Pritt MD. *Two-Dimensional Phase Unwrapping: Theory, Algorithms, and Software*. Wiley; 1998.

45. Mariappan YK, Glaser KJ, Ehman RL. Magnetic resonance elastography: A review. *Clin Anat*. 2010;23(5):497-511. doi:10.1002/ca.21006

46. Oliphant TE, Manduca A, Ehman RL, Greenleaf JF. Complex-valued stiffness reconstruction for magnetic resonance elastography by algebraic inversion of the differential equation. *Magn Reson Med*. 2001;45(2):299-310. doi:https://doi.org/10.1002/1522-2594(200102)45:2%3C299::AID-MRM1039%3E3.0.CO;2-O

47. Constantin D, Palierne JF, Freyssingeas É, Oswald P. High-frequency rheological behaviour of a multiconnected lyotropic phase. *Europhys Lett*. 2002;58(2):236. doi:10.1209/epl/i2002-00628-6

48. Nicolle S, Lounis M, Willinger R, Palierne JF. Shear linear behavior of brain tissue over a large frequency range. *Biorheology*. 2005;42(3):209-223.

49. P. Hébraud *, F. Lequeux † and, Palierne‡ JF. Role of Permeation in the Linear Viscoelastic Response of Concentrated Emulsions. ACS Publications. doi:10.1021/la001091g

50. Sango Solanas P, Tse Ve Koon K, Van Reeth E, Caussy C, Beuf O. Ultra-short echo time Magnetic Resonance Elastography. In: *Proc Int Soc Magn Reson Med; 2020; Abstract 168*.

51. Suzuki H, Tadano S, Goto M, Yamada S, Fujisaki K, Kajiwara I, Suga M, Nakamura G. Viscoelastic modulus of agarose gels by magnetic resonance elastography using Micro-MRI. *Mech Eng J*. 2015;2(3):14-00417-14-00417. doi:10.1299/mej.14-00417

52. Lefebvre PM, Tse Ve Koon K, Brusseau E, Nicolle S, Palieme JF, Lambert SA, Grenier D. Comparison of viscoelastic property characterization of plastisol phantoms with magnetic resonance elastography and high-frequency rheometry. In: *2016 38th Annual International Conference of the IEEE Engineering in Medicine and Biology Society (EMBC)*. IEEE; 2016:1216-1219. doi:10.1109/EMBC.2016.7590924

53. Aubry S, Risson JR, Kastler A, Barbier-Brion B, Siliman G, Runge M, Kastler B. Biomechanical properties of the calcaneal tendon in vivo assessed by transient shear wave elastography. *Skeletal Radiol*. 2013;42(8):1143-1150. doi:10.1007/s00256-013-1649-9

54. Hardy A, Rodaix C, Vergari C, Vialle R. Normal Range of Patellar Tendon Elasticity Using the Sharewave Elastography Technique: An In Vivo Study in Normal Volunteers. *Surg Technol Int*. 2017;31:227-230.

55. Burgio V, Civera M, Rodriguez Reinoso M, Pizzolante E, Prezioso S, Bertuglia A, Surace C. Mechanical Properties of Animal Tendons: A Review and Comparative Study for the Identification of the Most Suitable Human Tendon Surrogates. *Processes*. 2022;10(3):485. doi:10.3390/pr10030485

56. Manduca A, Bayly PJ, Ehman RL, Kolipaka A, Royston TJ, Sack I, Sinkus R, Van Beers BE. MR elastography: Principles, guidelines, and terminology. *Magn Reson Med*. Published online December 9, 2020. doi:10.1002/mrm.28627

57. Zhou B, Yang X, Zhang X, Curran WJ, Liu T. Ultrasound Elastography for Lung Disease Assessment. *IEEE Trans Ultrason Ferroelectr Freq Control*. 2020;67(11):2249-2257. doi:10.1109/TUFFC.2020.3026536

58. Aubry S, Nueffer JP, Tanter M, Becce F, Vidal C, Michel F. Viscoelasticity in Achilles Tendonopathy: Quantitative Assessment by Using Real-time Shear-Wave Elastography. *Radiology*. 2015;274(3):821-829. doi:10.1148/radiol.14140434

59. Drakonaki EE, Allen GM, Wilson DJ. Real-time ultrasound elastography of the normal Achilles tendon: reproducibility and pattern description. *Clin Radiol*. 2009;64(12):1196-1202. doi:10.1016/j.crad.2009.08.006

60. Dallaudière B, Trotier A, Ribot E, Verdier D, Lepreux S, Miraux S, Hauger O. Three-dimensional ultrashort echo time (3D UTE) MRI of Achilles tendon at 4.7T MRI with comparison to conventional sequences in an experimental murine model of spondyloarthropathy. *J Magn Reson Imaging*. 2019;50(1):127-135. doi:10.1002/jmri.26569

Tables

Table 1. Optimization parameters of the different OC pulses: excitation frequency f_{exc}, duration τ and relaxation times.

Pulse	f_{exc} (Hz)	τ (ms)	$T2_{opt}$ (ms)
A	300	7	2
B	600	5	2

Table 2. Pulse sequence parameters stablished for the acquisitions of every sample with the different methods. Geometry parameters were matrix of 128 x 128 pixels and FOV of 70 x 70 and 65 x 65 mm^2 for the *in vitro* and *ex vivo* acquisitions, respectively. The $MnCl_2$ phantom was characterized at 300 and 600 Hz. The tendon was only characterized at 600 Hz.

Phantom	f_{exc} (Hz)	Acquisitions	A (V)	f_{MEG} (Hz)	OC pulse	TE (ms)	TR (ms)	Acquisition time
1 & 5 mM $MnCl_2$	300	MEG MRE	1	300	-	12.5	300	38 s
	300	OC RARE		-	A	3.9	300	38 s
	300	OC UTE		-	A	0.07	300	8 min 2 s
	600	MEG MRE	1	600	-	8.3	300	38 s
	600	OC RARE		-	B	3.9	300	38 s
	600	OC UTE		-	B	0.07	300	8 min 2s
Tendon	600	MEG MRE	2	600	-	9.7	1500	3 min 12 s
	600	OC RARE		-	B	4.04	1500	3 min 12 s
	600	OC UTE		-	B	0.07	1500	40 min 12 s

Figures

Figure 1. Definition of the numerical phantom to solve the OC problem applied to MRE. Motion of spins induced by the shear wave is represented in dark blue oscillations. Note that two different vertical axes are considered.

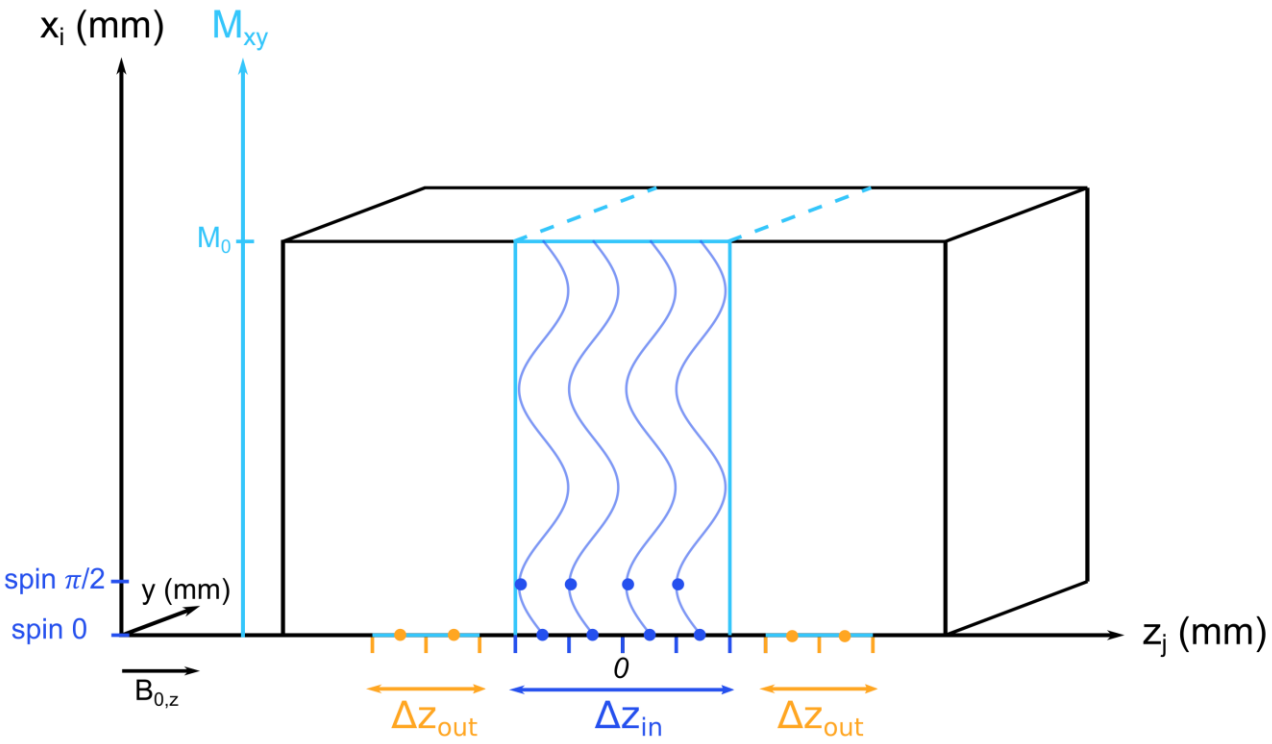

Figure 2. Sequence diagram of the OC UTE sequence used in this study. The OC pulse B (τ = 5 ms) is shown for illustration. The RF pulse and the magnetic field gradients are synchronised with the mechanical excitation and moved at each phase offset in order to sample the shear wave propagation.

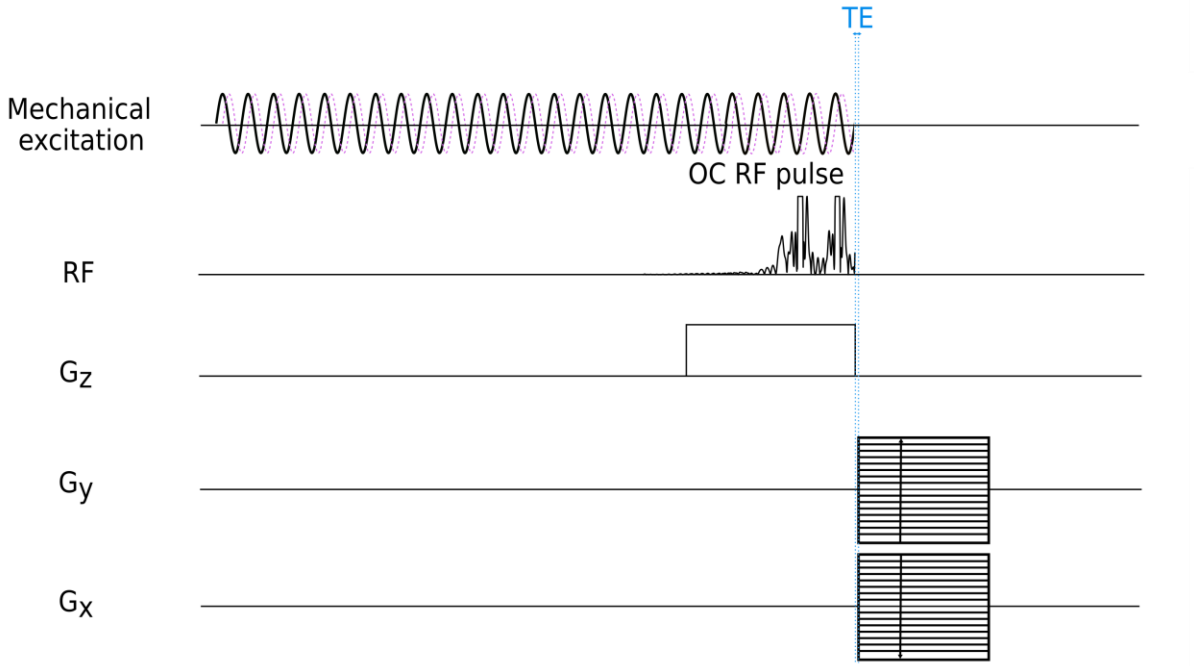

Figure 3. Characteristics of the OC pulse B: A) Simulated slice profile. The pink and green dashed lines represent the theoretical controlled slice thickness and outbands, respectively. B) Final transverse magnetization states in the Bloch sphere after the application of the OC pulse. The 0 (purple) and π/2 (green) isochromats are perfectly distinct. The group in the center (blue) represents the isochromats outside the controlled bandwidth.

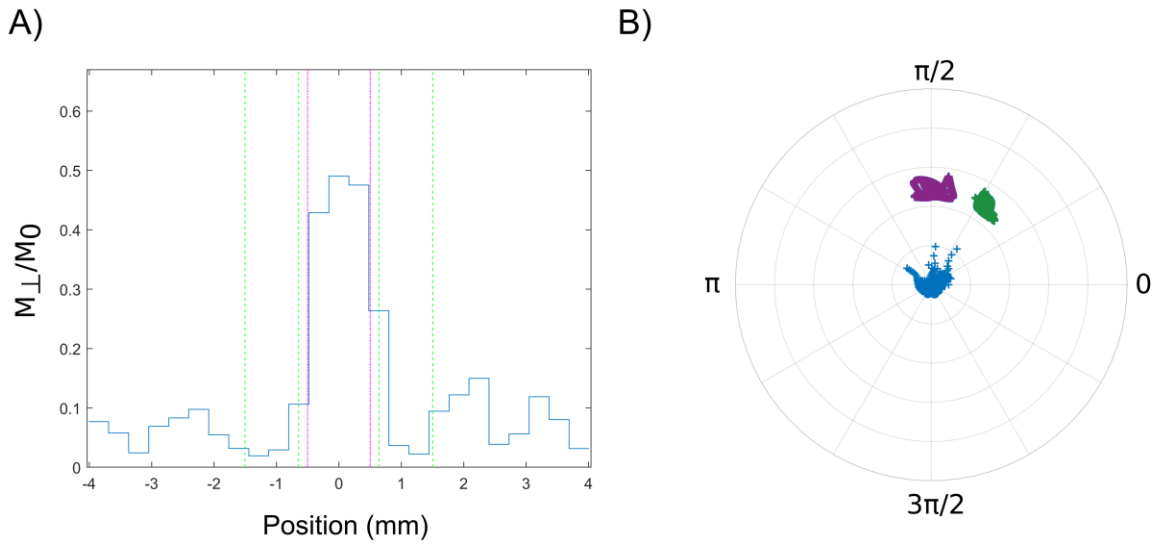

Figure 4. Numerical evaluation of the robustness of the OC pulse B with respect to the variability of the sample T2. Final magnetization states in the transverse plane after the application of the OC pulse and simulated slice profiles with and without motion for samples with T2 values of : A) 1 ms B) 20 ms. C) Transverse magnetization amplitude, simulated encoded phase and phase noise. D) PNR variation with respect to the sample T2 which varies between 0.2 and 20 ms.

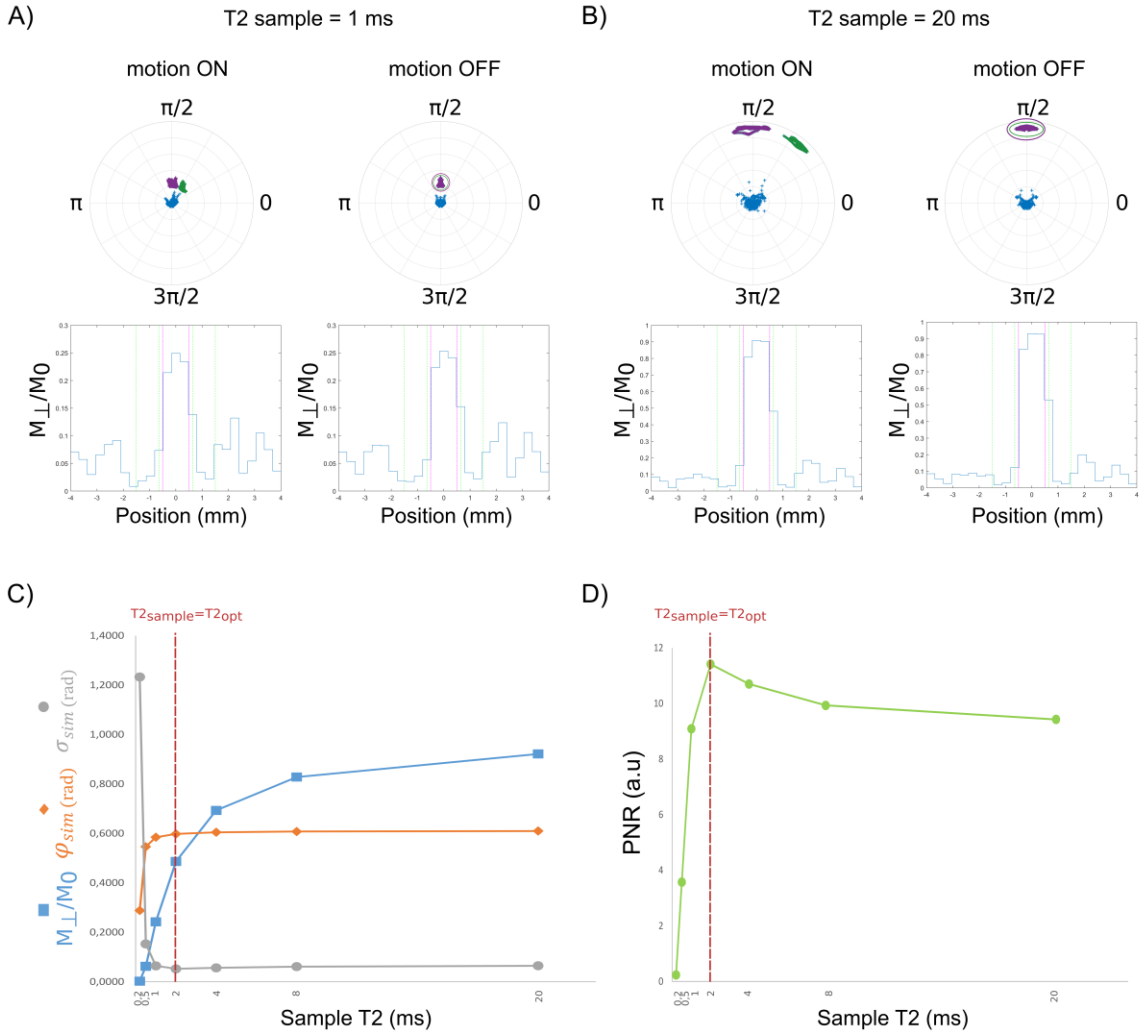

Figure 5. Magnitude (left colum), phase (central column) and shear storage modulus G' (right column) images obtained at 600 Hz with the different sequences : classical MEG MRE (top line), OC RARE (central line) and OC UTE (bottom line). For the OC sequences, pulse B was used. Both layers are delimited in magnitude images by dotted lines: the 5 and 1 mm MnCl2 concentration layer are located on the left and right, respectively.

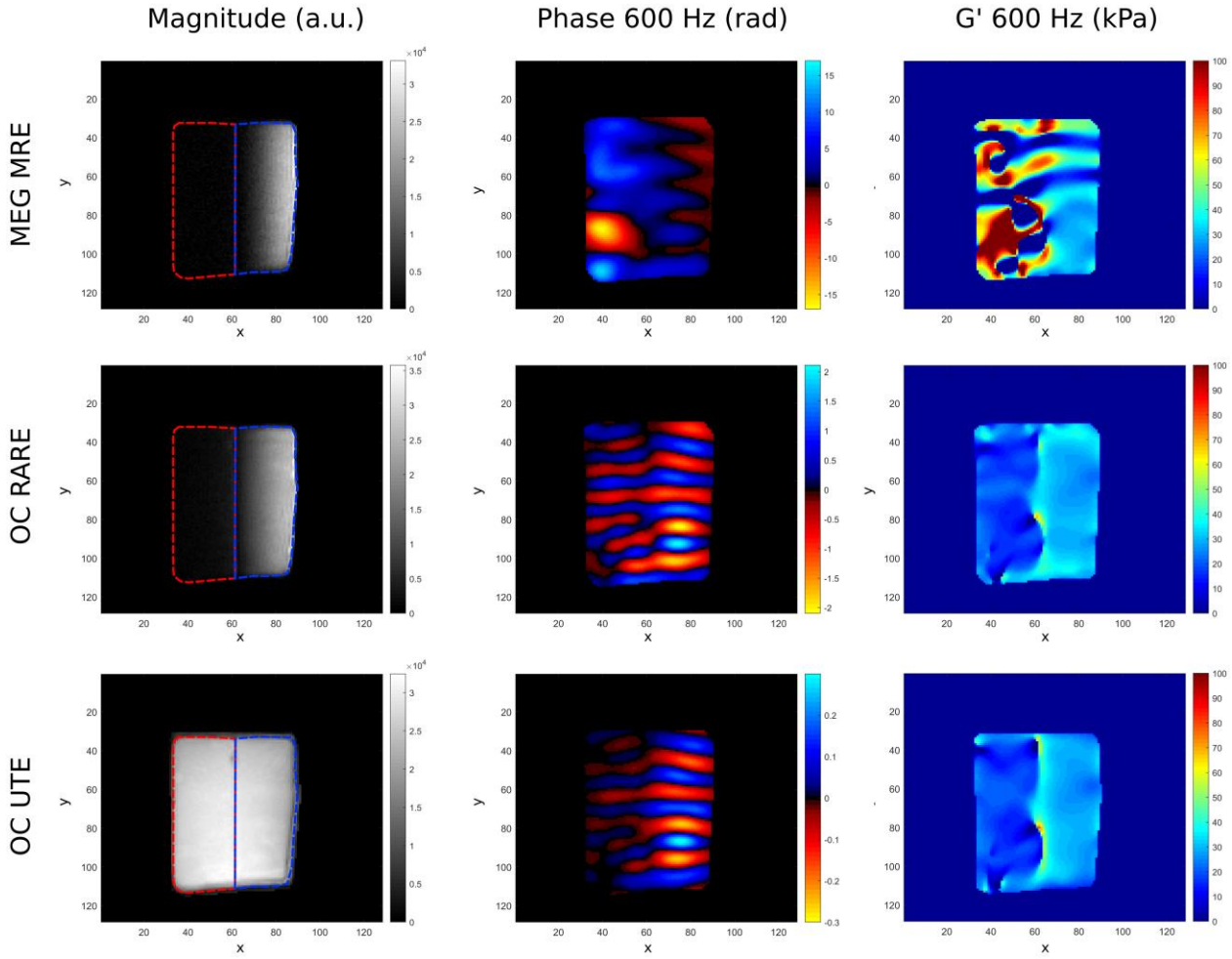

Figure 6. Results of phase encoding Δ, phase noise σ and Phase-to-Noise ratio PNR (in arbitrary units) obtained with the different acquisitions at multiple frequencies on the A) 5 mM and the B) 1 mM $MnCl_2$ concentration layers. Note that vertical axes are in logarithmic scale. Mean values and standard deviation of the shear storage modulus G' obtained for both excitation frequencies with the different sequences are presented on the C) 5 mM and the D) 1mM $MnCl_2$ concentration layers.

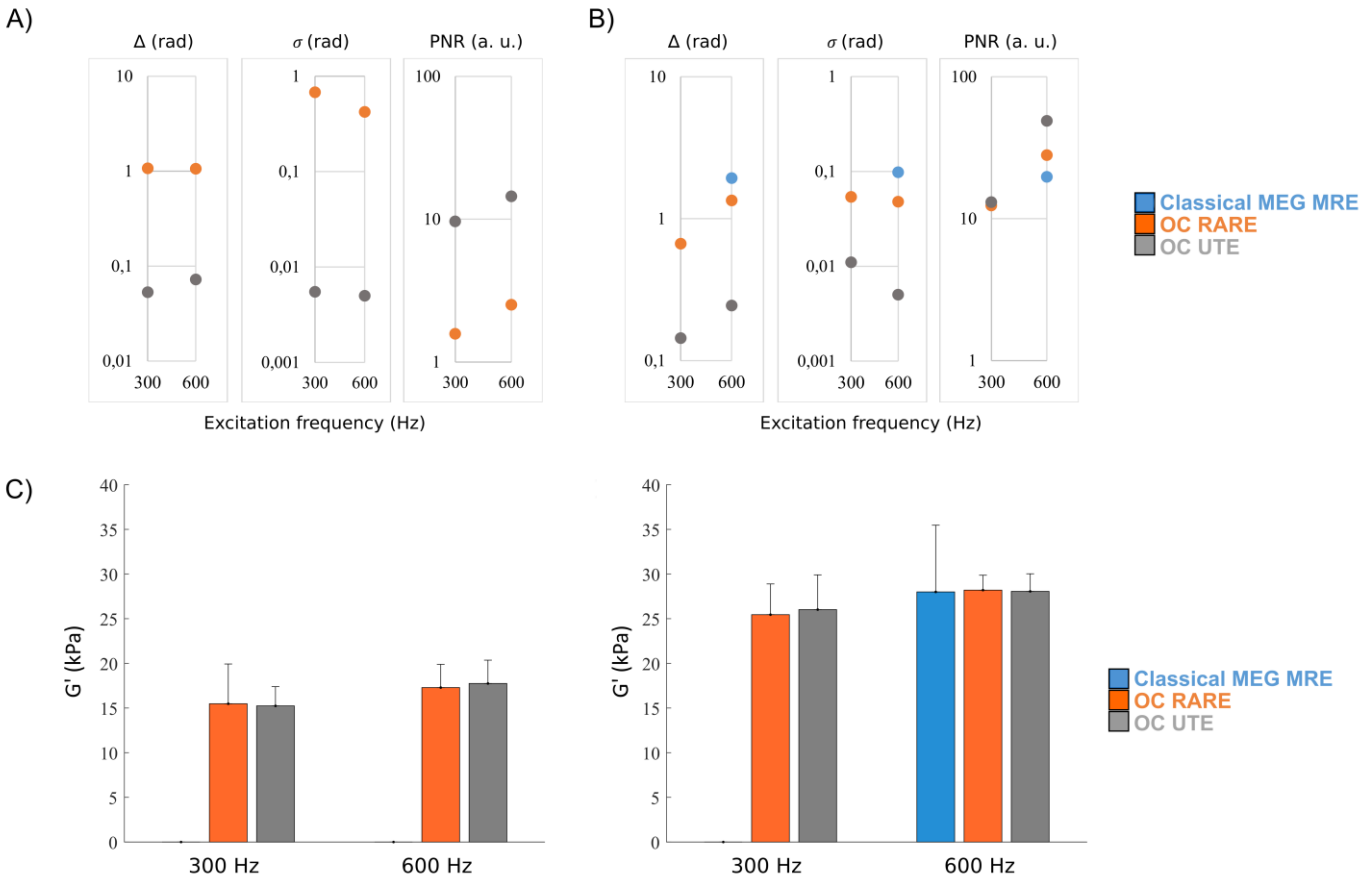

Figure 7. Magnitude images of the tendon with the A) Classical MEG MRE, B) OC RARE and C) OC UTE sequences. D) Phase image and E) elastogram obtained with the OC UTE sequence at 600 Hz on the tendon. G' mean value inside the ROI is 128 kPa.

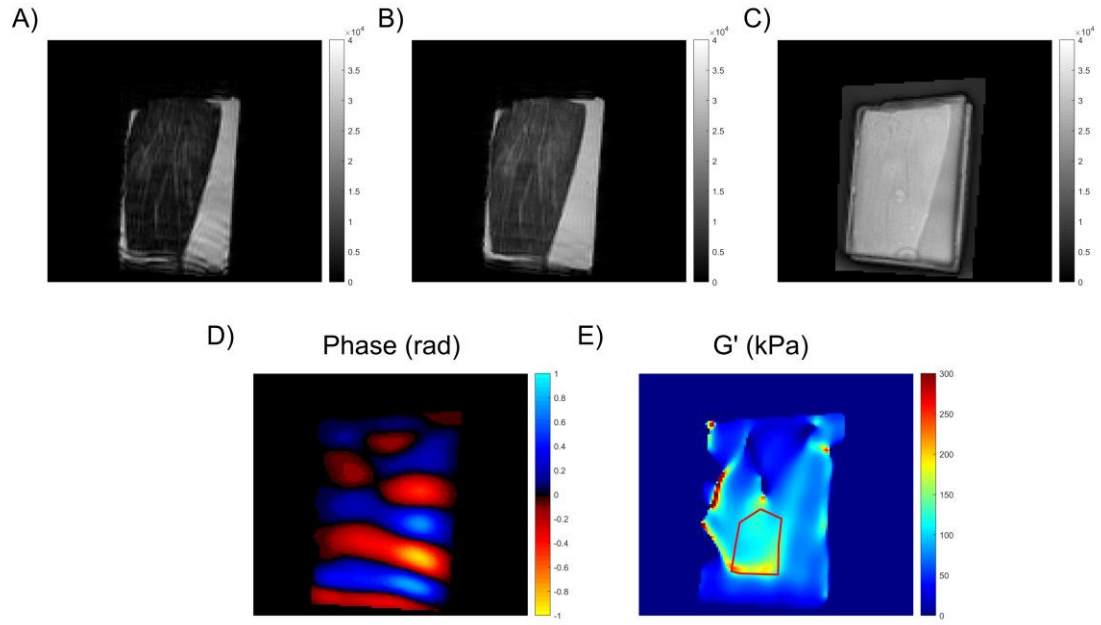

Figure 8. Shear storage modulus perpendicular to tendon fibers obtained by rheometry. Motion frequency varies from 10 to 630 Hz. Results are fitted to a power law (dotted line) whit a non linear least squares method on Matlab and the obtained trend equation is displayed on the figure (R^2 = 0.9836).